Structure of the Dodecahedral Penton Particle from Human Adenovirus Type 3

Article *in* Journal of Molecular Biology · March 2006

DOI: 10.1016/j.jmb.2005.11.048 · Source: PubMed

8 authors, including:

Patrizia Fuschiotti
University of Pittsburgh
51 PUBLICATIONS **1,025** CITATIONS
SEE PROFILE

Guy Schoehn
French National Centre for Scientific Research
292 PUBLICATIONS **9,889** CITATIONS
SEE PROFILE

Pascal Fender
French National Centre for Scientific Research
93 PUBLICATIONS **2,063** CITATIONS
SEE PROFILE

Sham Celine
The Hong Kong Polytechnic University
25 PUBLICATIONS **839** CITATIONS
SEE PROFILE

doi:10.1016/j.jmb.2005.11.048 J. Mol. Biol. (2006) 356, 510–520

JMB

Available online at www.sciencedirect.com

SCIENCE DIRECT®

ELSEVIER

Structure of the Dodecahedral Penton Particle from Human Adenovirus Type 3

P. Fuschiotti[1], G. Schoehn[2], P. Fender[3], C. M. S. Fabry[2], E. A. Hewat[1] J. Chroboczek[4], R. W. H. Ruigrok[2] and J. F. Conway[1]*

[1]*Laboratoire de Microscopie Electronique Structurale Institut de Biologie Structurale UMR 5075 CNRS-CEA-UJF 38027 Grenoble cedex, France*

[2]*Institut de Virologie Moléculaire et Structurale FRE 2854 CNRS-UJF, BP181 38042 Grenoble cedex 9, France*

[3]*Laboratoire d'Enzymologie Moléculaire, Institut de Biologie Structurale, UMR 5075 CNRS-CEA-UJF, 38027 Grenoble cedex, France*

[4]*Laboratoire de Biophysique Moléculaire, Institut de Biologie Structurale, UMR 5075 CNRS-CEA-UJF, 38027 Grenoble cedex, France*

**Corresponding author*

The sub-viral dodecahedral particle of human adenovirus type 3, composed of the viral penton base and fiber proteins, shares an important characteristic of the entire virus: it can attach to cells and penetrate them. Structure determination of the fiberless dodecahedron by cryo-electron microscopy to 9 Å resolution reveals tightly bound pentamer subunits, with only minimal interfaces between penton bases stabilizing the fragile dodecahedron. The internal cavity of the dodecahedron is ~80 Å in diameter, and the interior surface is accessible to solvent through perforations of ~20 Å diameter between the pentamer towers. We observe weak density beneath pentamers that we attribute to a penton base peptide including residues 38–48. The intact amino-terminal domain appears to interfere with pentamer–pentamer interactions and its absence by mutation or proteolysis is essential for dodecamer assembly. Differences between the 9 Å dodecahedron structure and the adenovirus serotype 2 (Ad2) crystallographic model correlate closely with differences in sequence. The 3D structure of the dodecahedron including fibers at 16 Å resolution reveals extra density on the top of the penton base that can be attributed to the fiber N terminus. The fiber itself exhibits striations that correlate with features of the atomic structure of the partial Ad2 fiber and that represent a repeat motif present in the amino acid sequence. These new observations offer important insights into particle assembly and stability, as well as the practicality of using the dodecahedron in targeted drug delivery. The structural work provides a sound basis for manipulating the properties of this particle and thereby enhancing its value for such therapeutic use.

Keywords: adenovirus; dodecahedron; penton; fiber; cryo-electron microscopy

Introduction

Adenoviruses are a large family of non-enveloped DNA viruses that infect a wide range of human and animal cell types, most commonly causing respiratory disease but also gastroenteritis or conjunctivitis. Their characteristic morphology includes an icosahedral capsid with a diameter of 900–1000 Å, pentameric capsomers (penton bases) at the vertices and hexavalent trimers (hexons) populating the facets in a pseudo-$T=25$ arrangement.[1] A trimeric fiber protein extends 100–300 Å (according to serotype) from the outer capsid surface and is attached non-covalently to each penton base forming the penton. Several other minor structural proteins are involved in stabilizing

Present addresses: P. Fuschiotti, Department of Immunology, University of Pittsburgh, Room E1040, Biomedical Science Tower, 200 Lothrop Street, Pittsburgh, PA 15261, USA; J. F. Conway, Department of Structural Biology, University of Pittsburgh, Room 2047, Biomedical Science Tower 3, 3501 5th Ave, Pittsburgh, PA 15260, USA.

Abbreviations used: Ad2, Ad3, Ad5, adenovirus serotypes 2, 3 and 5, respectively; Bs-Dd, dodecahedra constructed from adenovirus penton base protein alone; Pt-Dd, dodecahedra of pentons, i.e. penton base and fiber proteins; EM, electron microscopy; cryoEM, cryo-electron microscopy; Mab, monoclonal antibody.

E-mail address of the corresponding author: jxc100@pitt.edu

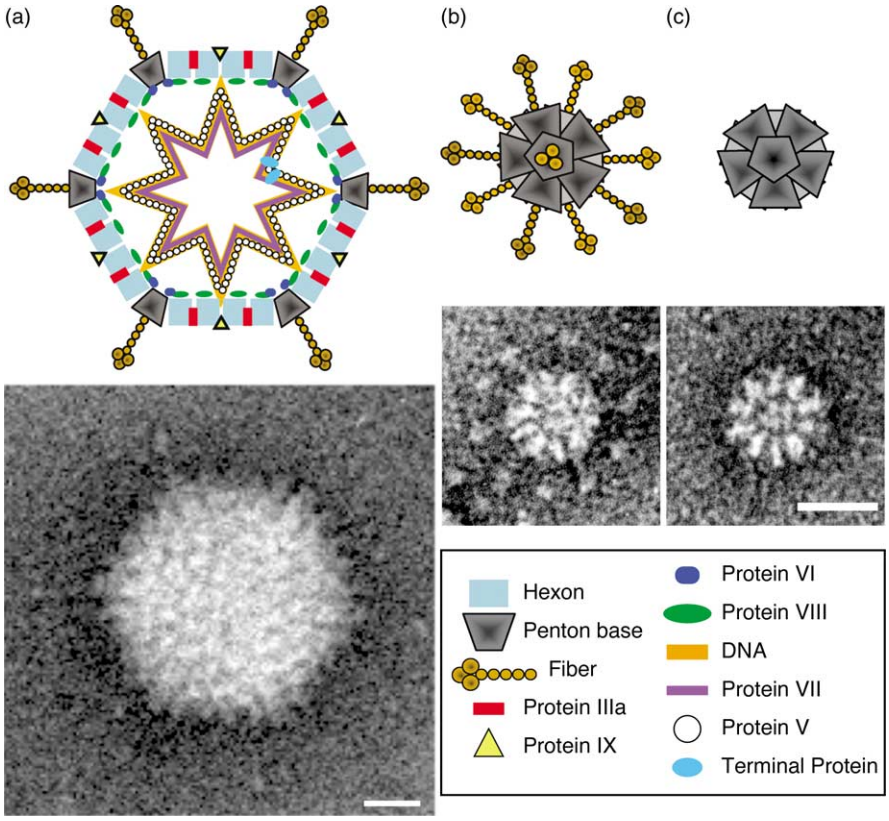

Figure 1. Schematics of adenovirus and its dodecahedron. (a) Diagram of adenovirus, including the major structural proteins: hexon (light blue), penton base (grey) and the trimeric fiber (gold) that extends outwards ending in a knob. Additional minor capsid proteins include the hexon "cementing" proteins IIIa (red bars), IX (yellow triangles), protein VIII associated with the hexons (green oval) and protein VI associated with the penton base (blue ovals). DNA is represented as an extended string (although in reality it is more compact than indicated here) and coated with associated proteins. Beneath is a negative-stain EM image of a viral particle. (b) Representation of the sub-viral dodecahedral particle with fiber bound (Pt-Dd) viewed down a 5-fold axis and a negative stain EM image from expressed penton base and fiber proteins where some fibers are visible, particularly the distal knobs. (b) The dodecahedral particle without fiber (Bs-Dd) and corresponding EM image. The bars represent 200 Å.

the capsid (Figure 1). The distal knob-domain of the fiber is necessary for cell recognition. Most subgroups (A–F, excluding B) bind the Coxsackie and adenovirus receptor (CAR),[2,3] an integral membrane protein of the tight junction in epithelial cells.[4] The interaction between the fiber and CAR is implicated both in viral entry and egress.[5] Several subgroup B adeno-viruses utilize another cell surface receptor, CD46,[6,7] but the primary receptor for another subgroup B member, adenovirus serotype 3 (Ad3), is still not known. Cell entry is gained by endocytosis, in most serotypes through RGD-loops extending from the penton base that bind to the αvβ3 or β5 integrins.[8,9] The penton base also has a role in release from endosomes and decapsidation.[10,11]

Models of the adenovirus capsid have been built by combining available crystallographic structures of the capsomers with lower resolution density maps of the entire capsid from cryo-electron microscopy (cryoEM). A model of the subgroup C Ad2 capsid was partially built from the trimeric hexon[12] and capsid reconstruction.[1] This model accounted for ~60% of the protein in the virion and offered insights into hexon–hexon and hexon–penton base interfaces, as well as indicating potential locations for some of the minor proteins. More recent updates include cryo-electron microscopy density maps of the Ad2 and Ad12 capsids to 21 Å resolution where surface features such as the RGD receptor binding loops were localized through binding MAbs or small receptor fragments.[13,14] However, much detail was lacking, including the structure of the penton base, its interaction with the fiber and the role of the symmetry-mismatch between these two components. Our recent cryoEM study on the Ad5 capsid has extended the resolution to 10 Å, allowing more detailed modeling of the capsomer interfaces and localization of minor structural proteins by comparison of native and deletion mutant capsids.[15]

For certain adenovirus serotypes, penton bases can self-assemble into a sub-viral particle called dodecahedron that comprises 12 copies of the penton arranged on a $T=1$ icosahedral lattice[16,17] and may include fiber molecules (penton dodecahedron, Pt-Dd) or not (base dodecahedron, Bs-Dd) (Figure 1). Analysis of the dodecahedral particle of Ad3 by cryoEM to a resolution of ~30 Å revealed

the overall shape of the particle and allowed an estimation of the dimensions of the internal cavity.[18] Comparison between particles including the fiber molecule (Pt-Dd) and those without (Bs-Dd) revealed apparent redistribution of density at the outermost surface of the penton at the presumed location of the mobile integrin-binding RGD loops. The fiber itself, however, was poorly resolved, possibly as a consequence of intrinsic flexibility, limited number of particles included in the reconstruction (30) or from bending imposed by a restricted depth of ice formed during preparation for microscopy. Subsequently, the dodecahedron was shown to enter cells efficiently using the same mechanism as adenovirus,[19,20] confirming the localization of the infection mechanisms to the penton's two constituent proteins, penton base and fiber. We have previously proposed the dodecahedron as an alternative to adenovirus for therapeutic delivery.[19,20] One of the potential advantages over the intact virus particle is that it cannot provoke infection directly or through recombination, as it harbors none of the viral genome. A second is the possibility of a weaker immune response compared to adenovirus because of its reduced protein content, thereby enhancing the success of multiple applications. In addition, recent work has shown that dodecahedra can penetrate a wider range of cells than the virus by entering through a heparin sulfate pathway.[21] However, the internal cavity of the dodecahedron is too small to accommodate more than ~100 bp of DNA and is thus too small to carry a gene, although it could accommodate drugs. Specific targeting to non-native receptors is possible through modification of the cell-recognition domains on the fiber, or combining fibers and penton bases from different adenovirus serotypes.[22]

Recently, a crystallographic model of the Ad2 penton base was reported. An expressed 48 N-terminal truncated form of the penton exposed to crystallization conditions lead to formation of dodecahedral particles in the crystal.[23] Interestingly, the full-length Ad2 penton base did not spontaneously form dodecahedra. The core of the structure is a jellyroll motif, an eight-stranded antiparallel β-barrel that is common to capsid proteins of certain virus families, with an extensive insertion of 308 residues (54% of the protein) between two β-strands of the jellyroll, and a second insertion of 54 residues between another pair of strands. The first insertion includes two external loops, one of which (the RGD loop) contains the integrin-binding RGD domain and is highly variable between serotypes in sequence and length. It is also flexible and none of the 74 residues of the loop were modeled in the crystal structure. The second loop (variable loop) is shorter, also variable between serotypes, and projects from the outer surface of the penton base into solvent. The binding pattern of the Ad2 fiber was revealed in a second dodecahedron structure including residues 11–21 from the N-terminal part of the fiber protein as five monomers bound to the penton base, albeit in non-stoichiometric quantities since the fiber molecule is a trimer.

The available adenovirus penton base protein sequences are highly conserved outside these external loops, suggesting that the bulk of the penton base has a common fold. The Ad2 penton protein differs in sequence from that of Ad3 at the amino terminus and at the two external loops, where the Ad3 protein is some 34 residues shorter in the RGD loop and nine residues longer in the variable loop. These three variable regions are perhaps the most important outside of the conserved interface residues that direct subunit and penton–hexon organization. The amino terminus is located internally to the capsid[15] and holds two conserved motifs of the form PPxY that may potentially interact with host cell ubiquitine ligases containing WW domains[24] presumably before incorporation into the capsid or after partial decapsidation. The RGD loop is a co-receptor binding site involved in endocytosis, and the second loop has unknown function but is clearly serotype specific.

Here we report on our work extending the structural characterization of the Ad3 dodecahedron by cryo-electron microscopy, including a more detailed visualization of the fiber and its interface with, and effects on, the penton base. We model the cryoEM density with the atomic coordinates of the Ad2 dodecahedron to compare the core structures and to identify the location of residues unique to the Ad3 penton sequence as well as part of the 48 amino-terminal residues not visualized by crystallography.

Results and Discussion

Although we published previously that dodecameric particles consisting of Ad3 penton base or Ad3 penton base plus fiber formed spontaneously upon expression,[18,20] new purification methods of recombinant protein produced in insect cells led to assembly of few particles, some incomplete, and with a much higher proportion of free penton bases (Figure 2(a)). We explain this discrepancy by first noting that the atomic structure of the Ad2 penton base dodecahedron was derived from protein that was N-terminally truncated, with the first 48 amino acid residues missing.[23] The internal space in this dodecahedron may be approximated by a sphere with diameter of 80 Å, sufficient to accommodate 225 kDa of tightly packed protein but which is too small to accommodate the 317 kDa of truncated peptides (60 copies of 48 residues). Clearly, dodecahedra cannot assemble from full-length penton base protein. Secondly, we observed that when full-length Ad3 penton base (Figure 2(c), lane 1) was kept for two weeks at room temperature, almost all the protein had assembled into dodecahedra (Figure 2(b)) and that the protein had been spontaneously degraded to a smaller size (Figure 2(c), lane 2). N-terminal sequencing showed

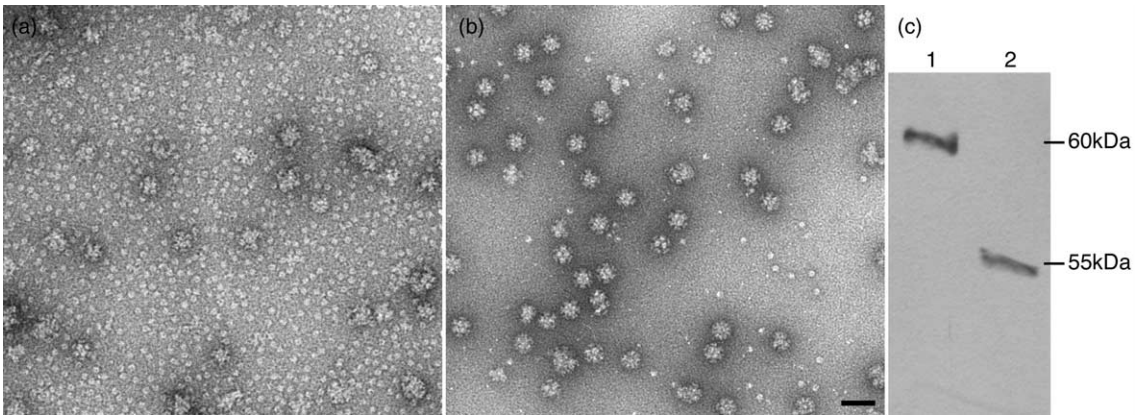

Figure 2. Negative stained images of expressed penton base. (a) Expressed penton base visualized immediately after expression and purification. Mainly free pentameric bases are visible with also some more or less complete dodecahedra. (b) Same sample as in (a) but visualized after two weeks at room temperature, having lost the first 37 residues. Most of the particles are well-formed dodecahedra. Only a few free penton bases are visible in the background. The scale bar represents 30 nm. (c) An SDS-PAGE gel of the two samples visualized in a, lane 1, and b, lane 2.

that the protein was N-terminally truncated between residues 37 and 38 (Figure 3). This 11 residue extension over the truncated Ad2 protein visualized by crystallography totals only 73 kDa (i.e. 60 copies of 11 residues) and is well able to pack into an 80 Å radius cavity. We conclude that our previous work on the Ad3 dodecahedron most probably involved N-terminally truncated protein resulting from inadvertent and unsuspected proteolysis. In the experiments shown here, all penton base protein was cleaved at the same site (residues 37–38), but in principle one would expect that dodecahedra could be formed from a mixture of cleaved and full-length protein.

The observation of dodecahedra in lysates of cells infected by Ad3[25] but not from cells infected by Ad2 may be due to the fact that the cleaved site is not conserved between the two serotypes (Figure 3) and

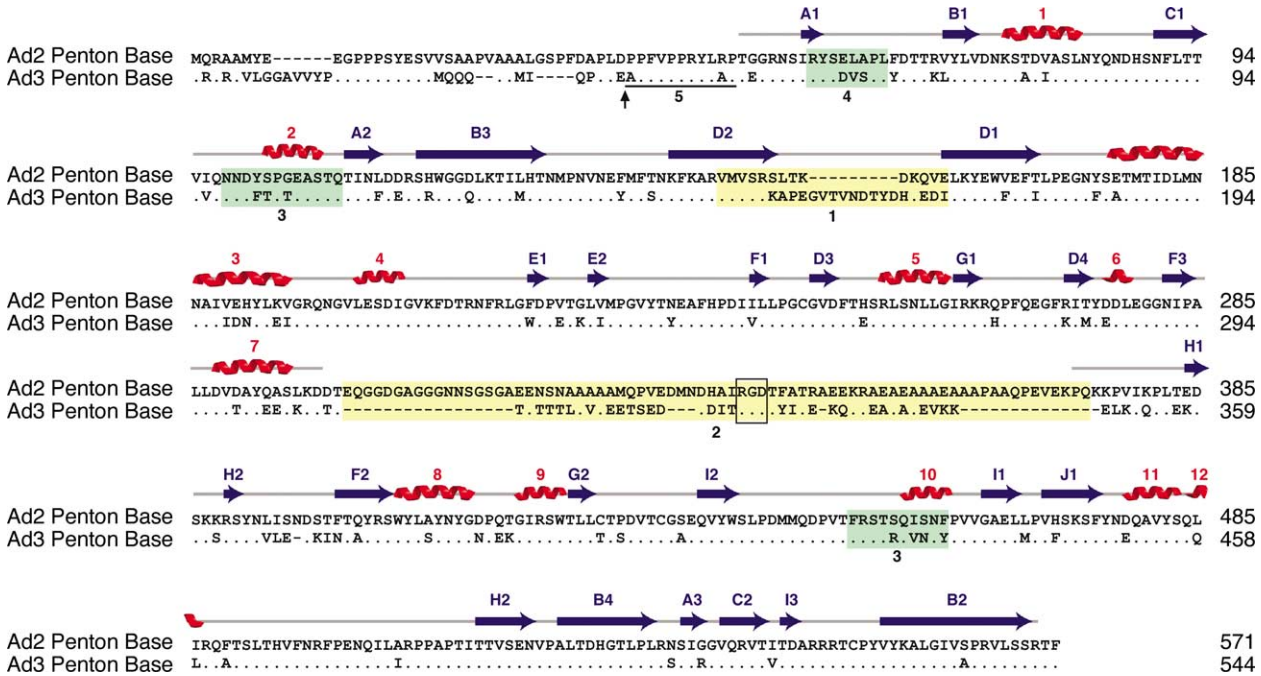

Figure 3. Sequence alignment of penton base proteins from human adenoviruses 2 and 3. Secondary structures in the Ad2 penton base are denoted above the sequence by blue arrows (β-strands) and red helices (α-helices). The RGD region (numbered 2, RGD is boxed into a black square) and the variable loop (numbered 1) are highlighted in orange whereas the regions involved in particle dodecamerization are in green and numbered 3 (two 2-fold related connections) and 4 (one connection on the 2-fold axis). The black arrow indicates the site of proteolysis allowing dodecahedron formation.[23] The number 5 and the black line above indicate residues 38–49 that are present in the Ad3 dodecahedron visualized in Figure 2(b) but not in the Ad2 dodecahedron X-ray structure. Regions 1–5 are also indicated in Figure 5.

that the Ad3 penton base is more readily cleaved in infected cells. During infection of cells by Ad2 there is production of a large excess of soluble fiber that is thought to be necessary to undo the tight junctions between cells involving the Ad2 receptor CAR.[5] Ad3 does not infect the same cells as Ad2 and uses a different receptor from CAR.[3] The fact that Ad3 dodecahedra are found in large quantities in Ad3-infected cells most likely means that these structures also play an as yet unknown role in the infection process.[26]

Electron cryo-microscopy and image analysis yielded models of the dodecahedron made from penton base only (Bs-Dd) and dodecahedron made of complete pentons (Pt-Dd) (Figure 4). The Bs-Dd particle was resolved at 9 Å but for the Pt-Dd particle only 16.5 Å was achieved as a consequence of both a smaller dataset of images as well as higher background noise due to the larger diameter particle being embedded in thicker ice. The Bs-Dd density map (Figure 4(d) and (e)) reveals tight packing of subunits in the penton bases but a looser association between penton bases. Although at lower resolution, the Pt-Dd map (Figure 4(f) and (g)) shows very strong density for the fiber up to the fiber head. Keeping in mind the improper imposition of 5-fold symmetry on the trimeric fiber molecule, several observations can be made. Firstly, the density level in the fiber is similar to that in the penton base, indicating that the fiber is coincident with the icosahedral 5-fold axis and so does not lose strength due to the imposed and inappropriate averaging. This strength of the fiber density is remarkable in comparison to that visualized in previous work[18] and likely results from embedding the particles in thicker ice, thus avoiding bending of the fibers, as well as correction of image distortions generated by the microscope (contrast transfer function).[27] We note that the Quantifoil grids used here appear to have rims of thick carbon around the holes that leads to thicker ice than for the "lacy" home made holey carbon films used previously. Secondly, we observe that the extent of the fiber is well delimited: small bridges of density connect it to the penton base (arrows in Figure 4(g)), and at the distal end the transition from strong to smeared density is sudden. Extending the radius of selection for the raw images does not result in any further extension of the fiber density in the reconstruction (results not shown), thus indicating the onset of either flexibility or a kink at the visible distal end. Such flexibility was observed before for negatively stained fibers of Ad2 that were seen to have a triangular shaped head with the fiber shaft lying flat on the carbon support film.[28] Flexibility of the fiber near the head and near the base probably assists in favorable positioning for receptor binding.[29] Finally, the fiber density shows an axial banding pattern with a spacing of about 15 Å. This feature will be discussed below.

The atomic structure of the Ad2 penton base was fit into the EM density maps of Ad3 Bs-Dd and Pt-Dd (Figure 5(a)–(d)). The atomic model fits very well (see Materials and Methods) apart from two loop areas where the EM density is too wide, as indicated in Figure 5(a) and (b) by 1 for the variable loop[15,23] and by 2 for the RGD loop (see also the sequence in Figure 3). The extra EM density in loop 1 is about 950 $Å^3$ in volume and can accommodate about 800 Da, slightly less than required for the eight amino acid insertion in the Ad3 penton base compared to that of Ad2. Less can be said about loop 2, the RGD loop, since most of it is invisible in the atomic structure of the Ad2 penton base[23] and in the 10 Å Ad5 structure.[15] Consequently, extra volume is visualized in the EM density maps corresponding to the RGD loop despite its shorter length than for Ad2 (Figure 3). This volume appears further from the penton's axis of symmetry in the Pt-Dd structure than for Bs-Dd, presumably a consequence of the fiber binding the penton base (see below).

The Ad3 dodecahedron is stabilized by three contacts between each pair of pentons. Two of these (marked 3 in Figure 5(c)–(f)) are related by the 2-fold axis and one (marked 4 in Figure 5(d) and (f)) is situated on the 2-fold axis. The corresponding positions in the Ad2 sequence are also marked by 3 and 4 in Figure 3. Because the quasi-atomic model of the Ad3 dodecahedron is made using the Ad2 X-ray structure, it is difficult to say exactly which amino acids interact across the Ad3 penton–penton interface. However, the atomic structure of the Ad2 penton base falls exactly inside the Ad3 EM density, implying that both types of penton base use the same structural elements to form the dodecahedron. Further, the high degree of homology between the sequences in these regions suggests that many of the same contacts may be made.

The EM structure shows additional density attached to the inside surface of the dodecahedron at the position of the N-terminal residue 49 of the Ad2 atomic structure (Figure 5(g) and (h); the N-terminal residue 49 is marked by an asterisk (*) and the extra density is marked by the number 5). We attribute this to the presence of 11 additional N-terminal residues present in the Ad3 penton base protein used for the cryoEM reconstructions, and it is a further indication that the N terminus of the penton base is sequestered inside the dodecahedron, and by inference inside the virus particle as well. Data obtained by cryoEM for the Ad5 capsid also showed extra density present under the penton and was likewise attributed to the N-terminal 48 residues of the penton base.[15] A corollary of these observations is that the N-terminal PPxY sequences that interact with cellular ubiquitine protein ligases[24,30] are not accessible in intact particles nor after assembly of new virus particles.

Model for the fiber density and its attachment to the base

The penton base is a pentamer but the fiber molecule that binds it is a trimer. There are five binding sites on the penton base for the N-terminal

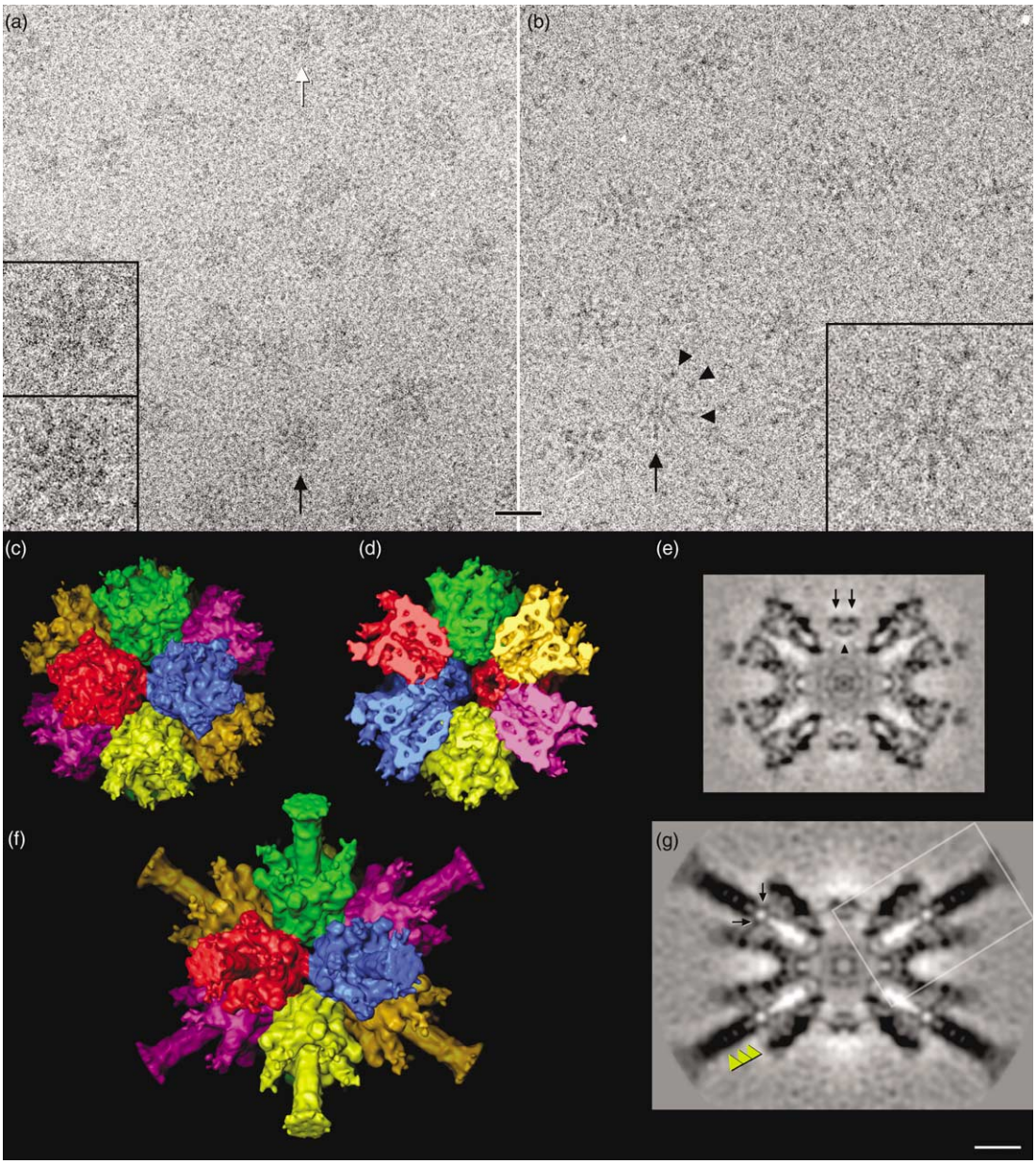

Figure 4. Structures of the Ad3 penton base dodecahedron with and without fiber. cryoEM images of Bs-Dd (a) and Pt-Dd (b), where arrowheads indicate fiber knobs. Several particles indicated by arrows are inset at double scale. The scale bar represents 250 Å. Surface representations of the Bs-Dd particle reconstruction viewed down a 2-fold axis and calculated from the cryoEM images are shown in (c), exterior view, and (d), interior view where the front half has been computationally removed. The penton bases are symmetrically identical, but colorized differently by a simple segmentation across the icosahedral 2-fold axes to aid in interpretation. The most peripheral density appears to be partially complete loops that may lose visibility due to flexibility. Gaps between penton bases are about 20 Å across and would allow solvent access to the interior. The interior cavity is about 80 Å in diameter and lined by the inwardly protruding loops of the penton bases. The central section corresponding to the sectioning plane in (d) is shown in grey-scale (protein is black) in (e). Densities 3 and 4 on the icosahedral 2-fold axis, and near or on the interface between penton bases, are marked with arrows and an arrowhead, respectively. These bridges are visualized in more detail in Figure 5. Equivalent views of the Pt-Dd particle are shown in (f), exterior view, and (g), central section, where density connections between the strong fiber density and the penton base are indicated with arrows. Also note the banding pattern along the axis of the fiber density, with a spacing of about 15 Å (yellow arrow heads). The boxed region is reproduced in Figure 6. An animation of the surface views is available on-line (Supplementary Data). The scale bar represents 50 Å.

tail of the fiber.[23] Therefore, when the fiber binds to the base, the fiber N termini will occupy at most three of the five available sites, an interesting example of symmetry mismatch but with unknown purpose. Because icosahedral symmetry is imposed upon the dodecahedron during the image reconstruction process, the density at the vertices, including that of the trimeric fiber, is 5-fold

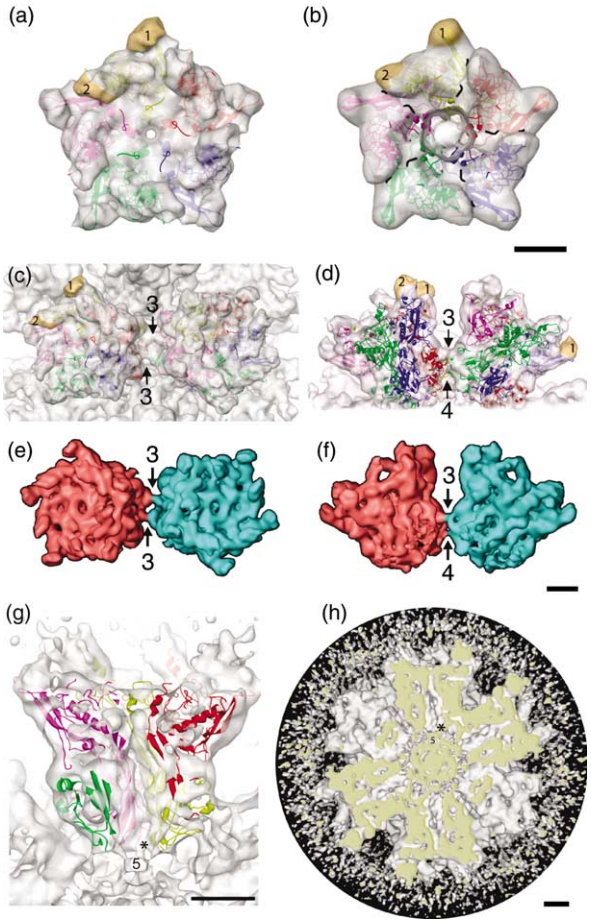

Figure 5. Quasi-atomic model of the Ad3 dodecahedron using the atomic structure of the Ad2 penton base. (a) Fit of the Ad2 penton base X-ray structure (PDB accession number 1X9P) into the Ad3 penton base EM density. The fit is nearly perfect at this resolution with only two unoccupied regions visible in the EM map. The first, marked 1, corresponds to the variable loop (see Figure 3) while the second, 2, is the RGD loop. (b) Fit of the fiber peptide, Ad2 penton base complex X-ray structure (PDB accession number 1X9T), into the Ad3 penton EM density. Extra densities are marked as in (a). The peptide that mimics the N terminus of the fiber (amino acid residues 10–20) is drawn in black. (c) and (d) Visualization of the contacts between two penton bases across the 2-fold axis. (c) Top-view along the icosahedral 2-fold axis, and (d) a perpendicular side view. The sequences involved in the different contacts are marked 3 and 4 as in Figure 3. Extra densities compared to the Ad2 X-ray structure are marked 1 and 2 as in (a) and (b). (e) and (f) The contact densities between penton bases are indicated in these surface views that have been rendered from a density map limited to 11 Å and contoured at a stringent level to highlight stronger densities. Arrows and numbers indicate features corresponding to those of (c) and (d) and in Figure 3. The boundaries between penton bases have been slightly adjusted from the simple 2-fold positions of Figure 4 by inspection of the density and respecting the 2-fold axis. The lower connection (4) is apparently weaker and is not quite continuous at this stringent contour level. (g) Same view of the Ad2 penton base X-ray data fitted into the Ad3 penton base as in (d) but the EM map is contoured at a lower threshold (i.e. more density is visible). It is then possible to see that the N-terminal part of the X-ray data (represented by an asterisk (*)) is now connected to a small cylindrical density inside the dodecahedron. We attribute this density to residues 38–49 (region 5 in Figure 3). (h) Same view as in (g) but for the entire dodecahedron. The cutting slice is colored in beige and region 5 and * are indicated under one penton base. The bars represent 25 Å.

averaged. When the EM density for Bs-Dd is subtracted from the density for Pt-Dd, several regions remain (colored light blue in Figure 6(a)), corresponding to the fiber as well as any penton base densities that are flexible in Bs-Dd but more rigid in Pt-Dd. On the top of the base, five spokes of density radiate azimuthally outwards, each consisting of three blobs. The center-most two blobs correspond to the density observed in the complete Ad5 capsid and also in the crystal structure of the Ad2 penton base plus an N-terminal fiber peptide, and are likely made up of Ad3 fiber residues 10-SFNPVYPYEDE-21.[15,23] The third blob is situated towards the outside of the penton base against the RGD loop and is either due to a stabilizing effect of the fiber N terminus on the flexible loop or comprises the nine N-terminal residues of the fiber tail. The volume of this blob of density, 1000 Å,^{3} can contain 850 Da of protein, enough for most of the nine N-terminal Ad3 fiber tail residues (1-MAKRARLST-9). In a previous analysis[18] we interpreted the volume difference between Bs-Dd and Pt-Dd near the RGD loop as movement by this loop because at the low resolution of that analysis we could only see that the midpoint of the mass of this loop changed position. Only higher resolution data would confirm our hypothesis about the identity of the outer-most blue blobs.

The cross-section of the EM density of the fiber in Figure 4(g) shows a series of striations along its length. The distances between these striations is 15(±2) Å and thus could correspond to the 15 amino acid pseudo-repeats in the fiber shaft.[28,31–33] Indeed, when the atomic structure of the distal shaft and knob region of the trimeric Ad2 fiber[31] is 5-fold averaged, a similar pattern of striations is observed from averaging of the repeating three pairs of antiparallel β-strands that are close to the fiber axis (Figure 6(b); β-strands and corresponding striations are arrowed). Analysis of the sequence of the Ad2 and Ad3 fibers shows that they have N-terminal tails of similar length (45 residues for Ad3 and 46 for Ad2) followed by three shaft repeats in common.[32] Although the short Ad3 fiber has only six repeats in total compared to the 22 for the longer Ad2 fiber,[32,34] the regular spacing of repeats can be directly compared with those of Ad2 that are present in the crystal structure of the fiber (Figure 6(b)). The cross-section of the fiber density of Ad3 Pt-Dd shows five clear bands, with the sixth striation from the last repeat being smeared out, as is the density for the knob, implying some flexibility is likely between the fifth and sixth repeat. The distance between the first striation and the inner-most blob of blue density shown in Figure 6(a) is about 15 Å and is evidently made up of the proline

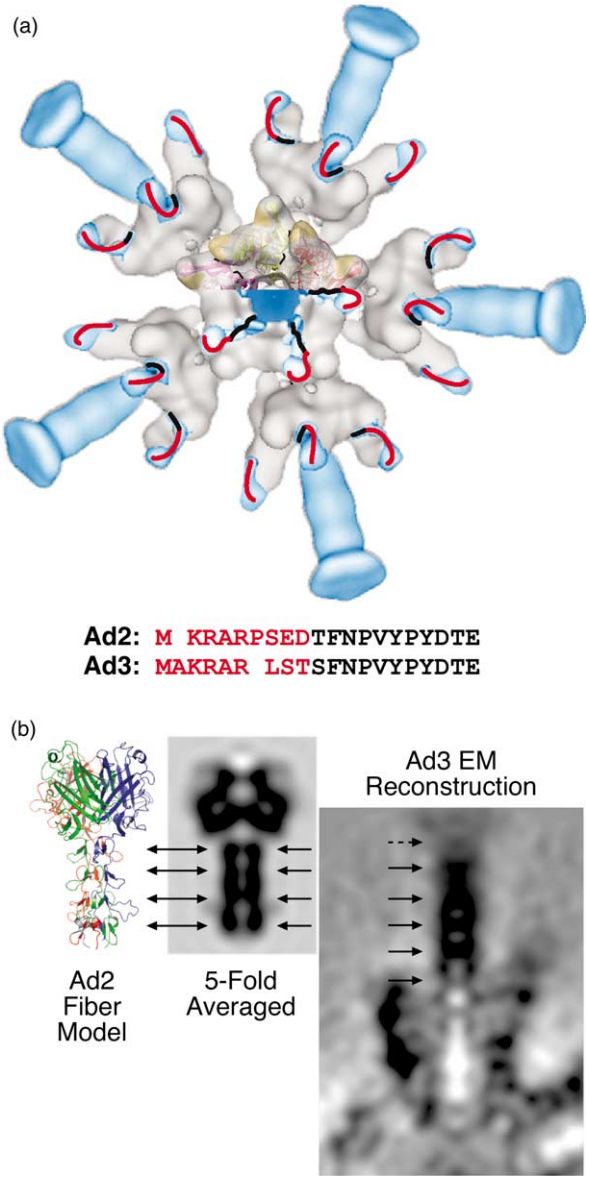

Figure 6. (a) The fiber of adenovirus. Difference mapping between Pt-Dd and Bs-Dd structures filtered at 18 Å resolution. Bs-Dd is in grey and the difference density is in blue. One half of the central penton shows the same fit as in Figure 5(b). The N-terminal fiber peptide (residues 11–21 of the Ad2 fiber[23]) is in black and superposes exactly with extra density visible in Pt-Dd (the two radially oriented cylinders of blue density). We interpret a third blue density localized on the outside part of the RGD loop (region 2 in Figures 3 and 5) as the N-terminal part of the fiber (Ad3 fiber residues 1–9) that is modeled by a red line connected to the black line (Ad2 fiber residues 11–21 seen in the crystal structure; Figure 5(b)). The sequence alignment of the first 20 amino acid residues of the Ad2 and Ad3 fibers indicates in black the amino acids that were modeled in the Ad2 crystallographic structure of the penton base with the bound fiber peptide, and in red those that were disordered. (b) Comparison of fiber density from the crystallographic structure of the Ad2 fiber head domain (residues 312–582)[31] as indicated, and from the Ad3 Pt-Dd density map. The Ad2 atomic model is averaged to mimic the Ad3 icosahedral reconstruction by filtering to 16 Å followed by imposition of 5-fold symmetry about an axis parallel with the fiber shaft. The section view shows four parallel striations corresponding to β-sheet crossovers, as indicated by arrows, and large loops between the lowest sets of β-sheet crossovers correspond to wisps of density between the lowest two striations in the section. At right is a corresponding section through the Ad3 fiber density of the Pt-Dd structure (boxed region from Figure 4(g)) and in approximate alignment by the distal ends presents similar striations. In the Ad3 fiber five striations are visible corresponding to five N-terminal motifs[32] while that for the distal sixth crossover is too smeared out to be clearly defined (broken arrow).

and glycine-rich sequence 21-SSSQHPFINPG FISPDGFTQSPNGV-45 that must form the well-defined link visible in the cross-section (Figure 4(g), arrows).

The loose packing between penton bases and the accessibility of the dodecahedron interior to solvent are features of the subviral particle that contrast sharply with the adenovirus capsid, where penton bases interact with hexon and other minor structural proteins to form a closed capsid. In addition, the insight into the need for truncation of the N-terminal 37 residues (48 for Ad2) in order to form dodecamers highlights another difference with the *in situ* penton base and has been crucial to understanding how to optimize particle production. These factors are important for our goal of developing the dodecahedron as a therapeutic vector (P.F. *et al*, unpublished results). Loose packing is more likely to allow our manipulation of the assembly status for the purpose of encapsidating a drug or other "cargo", although maintaining assembly buffer conditions will be crucial for particle stability. The large trefoil perforations also present an interesting challenge for retaining any packaged molecules, and clearly the size of the molecule must be sufficient to avoid diffusion through the pores. This may be achieved by polymerization of the molecules, thus increasing the diameter of the payload, or by modifying the interior surface of the dodecahedron cavity to attract the molecules but without affecting assembly. Finally, the need for truncation is essential for assembling particles in the first place, but also suggests that the amino termini might be suitable sites to introduce modifications for enhancing recruitment and retention of specific drugs and in sufficient quantity to be useful. Clearly much needs to be done to develop this system, but the structural work presented here gives some clear directions for future work.

Materials and Methods

Protein preparation

Adenovirus 3 dodecahedra were prepared using the baculovirus expression system as described.[20] Briefly, a double expression vector pAcUW31 (Clontech, Palo Alto, CA) was used for cloning the Ad3 penton base protein (60 kDa) and fiber protein (35 kDa) genes into the baculovirus genome. Infectivity titres were determined on monolayers of *Spodoptera frugiperda* (Sf21) cells by

standard procedures. *Trichoplusia ni* moth cells (High Five; Invitrogen) were infected with the recombinant baculovirus isolates at a multiplicity of infection of 5 plaque-forming units/cell. Lysates of infected High Five cells were separated on a 15%–40% (w/w) sucrose gradient containing 10 mM Tris–HCl, 150 mM NaCl, 10% glycerol, 2 mM EDTA (pH 6.6) for 18 h in a Beckman SW41 rotor at 40,000 rpm. Expressed protein was visualized by SDS-PAGE and Coomassie stain of the collected fractions at weights of 60 kDa and 35 kDa corresponding to the penton base protein and fiber protein, respectively. After the gradient, the protein-containing fractions localized in 38%–40% sucrose were dialyzed against 25 mM phosphate buffer (pH 6.6) and further purified by anionic exchange chromatography (Econo-Pac High Q Cartridge; BioRad) using a linear 0 to 1 M NaCl gradient in the phosphate buffer.

Electron microscopy

Particles were visualized by negative-stain EM to assess their assembly status using 1%(w/v) sodium silicotungstate (pH 7.0) as stain. cryoEM for structural analysis was performed according to standard low-dose methods. Bs-Dd particles were imaged on a JEOL JEM2010F microscope equipped with an Oxford CT3500 cryoholder operated at 200 kV and 50,000× nominal magnification. Pt-Dd particles were imaged with an FEI CM200 microscope with a Gatan 626 cryoholder operated at 200 kV and 38,000× nominal magnification. Quantifoil R2/1 grids (Quantifoil Micro Tools GmbH, Germany) were loaded with 4 μl of sample at 1 mg/ml, blotted and rapidly frozen in liquid ethane within a liquid nitrogen bath using a Zeiss cryo-plunger. Grids were maintained at liquid nitrogen temperatures during transfer into the microscope and imaged with low dose techniques on Kodak SO163 film. Fields were imaged twice at different defocus values with the closer-to-focus exposure being made first. Negatives were developed in full strength D19 for 12 min, screened by optical diffraction to reject those with weak or astigmatic power spectra, and digitized at a 7 μm sampling step on a Z/I Imaging PhotoScan (previously the Zeiss SCAI).

Image analysis

Particle images were selected manually from the digitized micrographs, corrected for contrast transfer function effects and processed as described[35] with several modifications as noted. The Bs-Dd micrographs (seven defocus pairs) yielded 5597 image pairs of which 1849 were selected for the final reconstruction; for Pt-Dd, 2141 image pairs were collected from six defocus pairs of micrographs, and 1071 were included in the final density map. Particle orientations were determined with the PFT protocol[36] with modifications (D.M. Belnap, J.B. Heymann & J.F.C., unpublished results), and three-dimensional density maps were calculated using Fourier–Bessel methods. Resolution was estimated by Fourier Shell Correlation[37] calculated between independent half-dataset maps, and applying a correlation limit of 0.3: for Bs-Dd this was at 9.3 Å and for Pt-Dd, 16.5 Å (see Supplementary Data, Figure 1). Density maps were manipulated with BSOFT utilities[38] and visualized with ROBEM (Rob Ashmore, Purdue University, Indiana), Amira (Mercury Computer Systems Inc, Merignac, France), and the UCSF Chimera software†. Density maps have been deposited in the Macromolecular Structure Database‡ with accession numbers 1178 for Bs-Dd and 1179 for Pt-Dd.

Docking of the atomic structure of the Ad2 penton base into the Ad3 penton base dodecahedron

The atomic structures of the Ad2 penton base alone (PDB accession number 1X9P) and in complex with the N-terminal fiber peptide (PDB accession number 1X9T) were fit into the EM model for Ad3 Bs-Dd and Pt-Dd, respectively. The atomic structures were placed manually into one penton base using the program O.[39] The optimization procedure was carried out using URO[40] with the pentamer treated as a single molecule (i.e. only applying icosahedral 2-fold and 3-fold symmetry). The scale factor was also optimized to determine the real magnification of the microscopes. For Bs-Dd the quality of the final fit is given by a correlation coefficient of 80.4%, a crystallographic *R* factor of 44.5% and a quadratic misfit of 17.9. The fitted scale factor was 0.98 of the original, corresponding to a calibrated pixel size in the cryoEM images of 1.37 Å. For Pt-Dd the quality of the final fit after masking out the fiber shaft and head domains is given by a correlation coefficient of 93%, a crystallographic *R* factor of 41.9% and a quadratic misfit of 14.9. The computed scale was 0.93 of the original, or 1.72 Å/pixel.

Difference imaging

Both the Bs-Dd and Pt-Dd maps were converted into SPIDER format,[41] adjusted to a common pixel size of 1.72 Å and subsequently filtered to 18 Å resolution. The two maps were then normalized (same min/max and standard deviation) and the correct threshold calculated to include the expected molecular mass of the particle (excluding the fiber for Pt-Dd). Pt-Dd was subtracted from Bs-Dd but no significant positive densities were visible (not shown). When Bs-Dd was subtracted from Pt-Dd, positive difference density resulted as seen in Figure 6(a).

Five-fold averaging of the fiber

The PDB file corresponding to the distal region of the Ad2 fiber (residues 319–582; PDB accession number 1QIU) was loaded into SPIDER and filtered to 16 Å. 5-fold symmetry was imposed along the fiber shaft to allow comparison with the corresponding density in the cryoEM model. A central slice through the resulting density is shown in Figure 6(b).

Acknowledgements

We thank Evelyne Gout for technical help, Dr Fred Metoz and Rémi Pinck for computational support, Drs David Belnap and Bernard Heymann for help with reconstruction software, and Dr Richard Wade for support and provision of microscopy equipment. J.F.C. acknowledges

† http://www.cgl.ucsf.edu/chimera/

‡ http://www.ebi.ac.uk/msd/

support from the CNRS through an ATIP grant and by a fellowship for P. F.

Supplementary Data

Supplementary data associated with this article can be found, in the online version, at doi:10.1016/j.jmb.2005.11.048

References

1. Stewart, P. L., Fuller, S. D. & Burnett, R. M. (1993). Difference imaging of adenovirus: bridging the resolution gap between X-ray crystallography and electron microscopy. *EMBO J*, **12**, 2589–2599.
2. Bergelson, J. M., Cunningham, J. A., Droguett, G., Kurt-Jones, E. A., Krithivas, A., Hong, J. S. *et al.* (1997). Isolation of a common receptor for Coxsackie B viruses and adenoviruses 2 and 5. *Science*, **275**, 1320–1323.
3. Roelvink, P. W., Lizonova, A., Lee, J. G., Li, Y., Bergelson, J. M., Finberg, R. W. *et al*. (1998). The coxsackievirus-adenovirus receptor protein can function as a cellular attachment protein for adenovirus serotypes from subgroups A, C, D, E, and F. *J. Virol.* **72**, 7909–7915.
4. Cohen, C. J., Shieh, J. T., Pickles, R. J., Okegawa, T., Hsieh, J. T. & Bergelson, J. M. (2001). The coxsackievirus and adenovirus receptor is a transmembrane component of the tight junction. *Proc. Natl Acad. Sci. USA*, **98**, 15191–15916.
5. Walters, R. W., Freimuth, P., Moninger, T. O., Ganske, I., Zabner, J. & Welsh, M. J. (2002). Adenovirus fiber disrupts CAR-mediated intercellular adhesion allowing virus escape. *Cell*, **110**, 789–799.
6. Gaggar, A., Shayakhmetov, D. M. & Lieber, A. (2003). CD46 is a cellular receptor for group B adenoviruses. *Nature Med.* **9**, 1408–1412.
7. Sirena, D., Lilienfeld, B., Eisenhut, M., Kalin, S., Boucke, K., Beerli, R. R. *et al*. (2004). The human membrane cofactor CD46 is a receptor for species B adenovirus serotype 3. *J. Virol.* **78**, 4454–4462.
8. Wickham, T. J., Mathias, P., Cheresh, D. A. & Nemerow, G. R. (1993). Integrins alpha v beta 3 and alpha v beta 5 promote adenovirus internalization but not virus attachment. *Cell*, **73**, 309–319.
9. Albinsson, B. & Kidd, A. H. (1999). Adenovirus type 41 lacks an RGD alpha(v)-integrin binding motif on the penton base and undergoes delayed uptake in A549 cells. *Virus Res.* **64**, 125–136.
10. Greber, U. F., Willetts, M., Webster, P. & Helenius, A. (1993). Stepwise dismantling of adenovirus 2 during entry into cells. *Cell*, **75**, 477–486.
11. Seth, P. (1994). Adenovirus-dependent release of choline from plasma membrane vesicles at an acidic pH is mediated by the penton base protein. *J. Virol.* **68**, 1204–1206.
12. Roberts, M. M., White, J. L., Grutter, M. G. & Burnett, R. M. (1986). Three-dimensional structure of the adenovirus major coat protein hexon. *Science*, **232**, 1148–1151.
13. Stewart, P. L., Chiu, C. Y., Huang, S., Muir, T., Zhao, Y., Chait, B. *et al*. (1997). Cryo-EM visualization of an exposed RGD epitope on adenovirus that escapes antibody neutralization. *EMBO J.* **16**, 1189–1198.
14. Chiu, C. Y., Mathias, P., Nemerow, G. R. & Stewart, P. L. (1999). Structure of adenovirus complexed with its internalization receptor, alphavbeta5 integrin. *J. Virol.* **73**, 6759–6768.
15. Fabry, C. M., Rosa-Calatrava, M., Conway, J. F., Zubieta, C., Cusack, S., Ruigrok, R. W. & Schoehn, G. (2005). A quasi-atomic model of human adenovirus type 5 capsid. *EMBO J.* **24**, 1645–1654.
16. Pettersson, U. & Hoglund, S. (1969). Sructural proteins of adenoviruses. 3. Purification and characterization of the adenovirus type 2 penton antigen. *Virology*, **39**, 90–106.
17. Norrby, E. (1968). Comparison of soluble components of adenovirus types 3 and 11. *J. Gen. Virol.* **2**, 135–142.
18. Schoehn, G., Fender, P., Chroboczek, J. & Hewat, E. A. (1996). Adenovirus 3 penton dodecahedron exhibits structural changes of the base on fibre binding. *EMBO J.* **15**, 6841–6846.
19. Fender, P., Schoehn, G., Foucaud-Gamen, J., Gout, E., Garcel, A., Drouet, E. & Chroboczek, J. (2003). Adenovirus dodecahedron allows large multimeric protein transduction in human cells. *J. Virol.* **77**, 4960–4964.
20. Fender, P., Ruigrok, R. W., Gout, E., Buffet, S. & Chroboczek, J. (1997). Adenovirus dodecahedron, a new vector for human gene transfer. *Nature Biotechnol.* **15**, 52–56.
21. Vives, R. R., Lortat-Jacob, H., Chroboczek, J. & Fender, P. (2004). Heparan sulfate proteoglycan mediates the selective attachment and internalization of serotype 3 human adenovirus dodecahedron. *Virology*, **321**, 332–340.
22. Mizuguchi, H. & Hayakawa, T. (2004). Targeted adenovirus vectors. *Hum. Gene Ther.* **15**, 1034–1044.
23. Zubieta, C., Schoehn, G., Chroboczek, J. & Cusack, S. (2005). The structure of the human adenovirus 2 penton. *Mol. Cell*, **17**, 121–135.
24. Galinier, R., Gout, E., Lortat-Jacob, H., Wood, J. & Chroboczek, J. (2002). Adenovirus protein involved in virus internalization recruits ubiquitin-protein ligases. *Biochemistry*, **41**, 14299–14305.
25. Norrby, E. (1969). The structural and functional diversity of Adenovirus capsid components. *J. Gen. Virol.* **5**, 221–236.
26. Fender, P., Boussaid, A., Mezin, P. & Chroboczek, J. (2005). Synthesis, cellular localization, and quantification of penton–dodecahedron in serotype 3 adenovirus-infected cells. *Virology*, **340**, 167–1673.
27. Conway, J. F. & Steven, A. C. (1999). Methods for reconstructing density maps of "single" particles from cryoelectron micrographs to subnanometer resolution. *J. Struct. Biol.* **128**, 106–118.
28. Ruigrok, R. W., Barge, A., Albiges-Rizo, C. & Dayan, S. (1990). Structure of adenovirus fibre. II. Morphology of single fibres. *J. Mol. Biol.* **215**, 589–596.
29. Wu, E., Pache, L., Von Seggern, D. J., Mullen, T. M., Mikyas, Y., Stewart, P. L. & Nemerow, G. R. (2003). Flexibility of the adenovirus fiber is required for efficient receptor interaction. *J. Virol.* **77**, 7225–7235.
30. Chroboczek, J., Gout, E., Favier, A. L. & Galinier, R. (2003). Novel partner proteins of adenovirus penton. *Curr. Top. Microbiol. Immunol.* **272**, 37–55.
31. van Raaij, M. J., Louis, N., Chroboczek, J. & Cusack, S. (1999). Structure of the human adenovirus serotype 2 fiber head domain at 1.5 Å resolution. *Virology*, **262**, 333–343.
32. Chroboczek, J., Ruigrok, R. W. & Cusack, S. (1995). Adenovirus fiber. *Curr. Top. Microbiol. Immunol.* **199**, 163–200.
33. Green, N. M., Wrigley, N. G., Russell, W. C., Martin, S. R. & McLachlan, A. D. (1983). Evidence for a repeating

cross-beta sheet structure in the adenovirus fibre. *EMBO J.* **2**, 1357–1365.
34. Signas, C., Akusjarvi, G. & Pettersson, U. (1985). Adenovirus 3 fiber polypeptide gene: implications for the structure of the fiber protein. *J. Virol.* **53**, 672–678.
35. Conway, J. F. & Steven, A. C. (1999). Methods for reconstructing density maps of single particles from cryo-electron micrographs to subnanometer resolution. *J. Struct. Biol.* **128**, 106–118.
36. Baker, T. S. & Cheng, R. H. (1996). A model-based approach for determining orientations of biological macromolecules imaged by cryoelectron microscopy. *J. Struct. Biol.* **116**, 120–130.
37. van Heel, M. (1987). Similarity measures between images. *Ultramicroscopy*, **48**, 95–100.
38. Heymann, J. B. (2001). Bsoft: image and molecular processing in electron microscopy. *J. Struct. Biol.* **133**, 156–169.
39. Jones, T. A., Zou, J. Y., Cowan, S. W. & Kjeldgaard, M. (1991). Improved methods for building protein models in electron density maps and the location of errors in these models. *Acta Crystallog. sect. A*, **47**, 110–119.
40. Navaza, J., Lepault, J., Rey, F. A., Alvarez-Rua, C. & Borge, J. (2002). On the fitting of model electron densities into EM reconstructions: a reciprocal-space formulation. *Acta Crystallog. sect. D*, **58**, 1820–1825.
41. Frank, J., Radermacher, M., Penczek, P., Zhu, J., Li, Y., Ladjadj, M. & Leith, A. (1996). SPIDER and WEB: processing and visualization of images in 3D electron microscopy and related fields. *J. Struct. Biol.* **116**, 190–199.

Edited by Sir A. Klug

(Received 7 September 2005; received in revised form 4 November 2005; accepted 15 November 2005)
Available online 9 December 2005